Schweizerische Eidgenossenschaft
Confédération suisse
Confederazione Svizzera
Confederaziun svizra

Eidgenössisches Departement für
Umwelt, Verkehr, Energie und Kommunikation UVEK

Bundesamt für Energie BFE

Jahresbericht 31. August 2009

Development of wind turbines for safe operation in alpine environments

LEC
Laboratory for Energy Conversion

ETH
Eidgenössische Technische Hochschule Zürich
Swiss Federal Institute of Technology Zurich

Auftraggeber:
Bundesamt für Energie BFE
Forschungsprogramm Windenergie
CH-3003 Bern
www.bfe.admin.ch

Auftragnehmer:
Laboratory for Energy Conversion
ETH Zürich MLJ33
Sonneggstrasse 3
CH-8092 Zürich
www.lec.ethz.ch

Autoren:
Sarah Barber, Laboratory for Energy Conversion, ETH Zürich, barbers@ethz.ch
Reza Abhari, Laboratory for Energy Conversion, ETH Zürich, abhari@ethz.ch

BFE-Bereichsleiter: Katja Maus
BFE-Programmleiter: Robert Hobarty
BFE-Vertrags- und Projektnummer: 153536 / 102744

Contents

Abstract

Many favourable sites for wind farms, particularly in the Swiss Alps, are located in cold, wet regions where the build-up of ice is a risk and therefore limits the installation of wind turbines. The aim of this work is to quantify and understand in detail the effects of blade icing on wind turbine performance and to propose mitigation strategies. The project is unique in that it is carried out using a multi-disciplinary approach that combines (1) analysis of field data, (2) controlled experiments on a sub-scale wind turbine model and (3) 3D Computational Fluid Dynamics. In part (1) the wind data and full-scale wind turbine power and icing measurements from the Alpine Test Site Gütsch over one year are analysed. Icing on the blades is estimated to cause approximately a 2% loss in Annual Energy Production (AEP). Other losses due to the particular location of the turbine in complex terrain are found to reduce the expected AEP by up to 23%. These major losses must be further investigated in controlled experiments. The analysis of photographs of ice on the blades, alongside numerical simulations, enables five ice geometries to be defined for Gütsch atmospheric conditions (2331 m altitude). One further “extreme” ice shape is also defined, which is representive of ice formed on wind turbines installed at lower altitude sites such as the Bern Jura (800 – 1500 m). In part (2), experiments are undertaken in the new sub-scale wind turbine test facility at ETH Zürich using a novel method to quantify performance. The defined ice shapes are attached to the blades and the performance compared. The five shapes representative of the ice formed at Gütsch are found to reduce the Annual Energy Production by up to 2%. However, the “extreme” ice shape could result in a loss in Annual Energy Production of up to 17%. Furthermore, the presence of ice on the most outboard 5% of the blade is found to be key to performance. Ice removal or prevention systems could be substantially more efficient if their effectiveness was tailored for the outboard 5% of the blade. Additionally, a new dedicated Fast Response Aerodynamic Probe measuring system has been installed at the facility. Initial measurements prove its ability to resolve key flow features behind the wind turbine rotor. Part (3) of the project involves the Computational Fluid Dynamics analysis of the defined ice geometries on the rotor blades. The changes in performance match well with the experimental measurements. It is found that separation over the entire blade span is the cause for the major losses in power measured for the “extreme” ice shape. A predictive tool that developers of wind energy projects located in regions that are highly susceptible to icing can use for project development, which identifies the locations where “extreme” ice formation is a risk, would be highly beneficial to wind farm developers in Switzerland.

Zusammenfassung

Potentielle Standorte von Windkraftwerken liegen häufig in kalten Gebieten, wo die Wahrscheinlichkeit von Eisbildung erhöht ist, was keine einfachen Bedingungen für Windturbinen darstellt. Das Ziel dieses Projektes ist, die Effekte von Rotorblatteisbildung auf die Leistung einer Windkraftanlage experimentell und numerisch zu untersuchen und abhelfende Massnahmen für die Hindernisse vorzuschlagen. Das Projekt wird basierend auf der Kombination dreier interdisziplinärer Vorgehensstrategien durchgeführt: der Felddatenanalyse (1), kontrollierten Messungen an einem Modell einer Windenergieanlage in einem Wasserschlepptank (2), und 3D Computational Fluid Dynamics (3). Im Rahmen von (1) wurden die Windgeschwindigkeits-, Anlageleistungs- und Vereisungsdaten über ein Jahr der Versuchswindkraftanlage am *Alpine Test Site Gütsch* analysiert. Jahresenergieertragverluste (AEP) bis 2% wurden von Rotorblatteisbildung verursacht. Für Verluste bis 23% ist komplexes Gelände verantwörtlich, was anhand kontrollierter Versuche weiterer Erforschung bedarf. Fünf verschiedene für die Schaufelvereisung relevante Formen wurde für die atmosphärischen Bedingungen am Gütsch (2,331 m ü.M.) anhand Fotoananalyse und numerischer Simulationen bestimmt. Eine weitere “extreme” Eisform wurde identifiziert, die die Eisbildung an Windkraftanlagen an tiefer gelegenen Standorten wie im Berner Jura (800 – 1500 m ü.M.) repräsentiert. In (2) wurden experimentelle Versuche im *ETHZ sub-scale model wind turbine test facility* durchgeführt. Eine neue Methode für die Quantifizierung der Leistung wurde entwickelt. Die oben beschriebenen Eisformen wurden an den Rotorblättern befestigt und bezüglich resultierender Leistung der Turbine untereinander verglichen. Auch in dieser Versuchseinrichtung wurde ein Jahresenergieertragsverlust von 2% ermittelt, der auf die fünf Eisformen zurückzuführen ist. Die “extreme” Form führt jedoch zu Jahresenergieertragverlusten bis 17%. Besonders kritisch für die Verluste in der Energieerzeugung ist die Vereisung der äusseren 5% der Blattlänge. Der Einsatz von Eisentfernungs- und Eisverhütungsgeräten wäre viel effizienter, wenn er nur auf diesen Teil zugeschnitten wäre. Anschliessend wurde ein neues angepasstes Fast Response Aerodynamic Probe Messsystem an der Versuchseinrichtung installiert. Die ersten Messungen bestätigen die Eignung des Systems, die wichtigsten Strömunsgrundzüge hinter dem Rotor aufzulösen. Der letzte Teil (3) beinhaltet die Computational Fluid Dynamics Analyse der Eisformen auf den Rotorblättern. Die simulierten Leistungsänderungen bestätigen die experimentellen Messwerte. Es wurde somit bewiesen, dass die Ablösung an der ganzen Blattlänge die Ursache für die grössen Leistungsverluste der “extremen” Eisform ist. Ein Tool für die Bestimmung der “extremen” Eisbildung an potentiellen Windkraftanlagestandorten wäre höchst nützlich für Entwicklungsunternehmer in der Schweiz.

1. Introduction

Wind energy is the world's fastest growing source of electricity production, and a key source of clean, plentiful energy for the future. In order for wind energy to fully reach its potential, the wind rich sites must be effectively taken advantage of. As the power output of a given wind turbine is proportional to the cube of the wind velocity, a site's capacity is highly dependent on the wind speed.

Many favourable sites for wind farms in terms of high wind speeds are located in cold, wet regions such as the Swiss Alps. In these regions the installation of wind turbines is limited due to problems of ice formation, both on instrumentation and on the blades. Power curve predictions can be of low accuracy, and the actual performance often deviates significantly from the expected performance. The improved understanding and quantification of these losses is vital for wind farm developers and investors, who must estimate accurately the expected energy production of a project in order to quantify its risks and assess its financial viability.

The formation of ice on airfoils is generally known to have a detrimental effect on their lift coefficient (C_L) and drag coefficient (C_D) performance. Icing on aircraft wings has been well documented, and using icing wind tunnels (Broeren *et al.*, 2006) and numerical simulation (Bragg *et al.*, 2007) C_L was found to reduce by up to 30% and C_D was found to increase up to 50%. The effect of icing on wind turbine blades has been less studied (Bose, 1992). Power losses due to icing have been estimated to be up to 20% using 2D Computational Fluid Dynamics (CFD) and Blade Element Momentum (BEM) methods (Brahimi *et al.*, 1998).

The present work is a combined analytical, experimental and computational study of the effects of icing on wind turbine performance and aerodynamics. It aims to lead to improved understanding and quantification of the losses due to blade icing in order to help wind turbine development and optimisation.

The specific objectives are to,

- assess the effects of icing on the performance of a full-scale wind turbine that operates in potential icing conditions;
- understand and quantify the effects of ice formation on wind turbine blades, using the laboratory's new sub-scale wind turbine test facility and novel performance measurement technique;
- detail the flow-field around 3D, rotating wind turbine blades with representative ice shapes on the blades using Computational Fluid Dynamics.

Each of these objectives are addressed separately in this report, followed by a discussion of the results and their consequences.

2. Full-scale wind turbine performance

2.1 Summary of data analysis

In the first part of the project, the performance of the wind turbine at the Alpine Test Site Gütsch, a variable pitch and variable speed wind turbine located in complex terrain with the potential for ice formation, was analysed using 10-min averaged data over a year (from Meteotest). Velocity and density corrections were applied to the measured power and velocity data. Details of the analysis can be found in the Progress Report of this project (Barber, 2008).

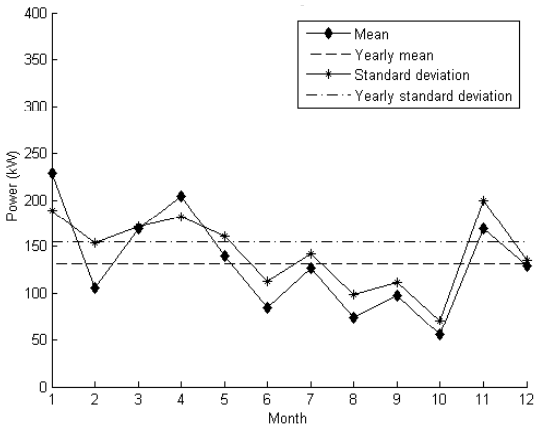

The frequency spectrum of the data shows significant variations in wind speed at the site of the order of a month, and the monthly power output and energy production were found to vary up to 75% and 50% between months, respectively. The variation in monthly power output is shown in Fig. 1.

Figure 1. Power output vs. month.

The standard IEC bin-averaged power and power coefficient curves were estimated for the measured data (IEC, 1998). The power curve was highly scattered due to the complex terrain, and its mean deviation from the standard manufacturer's curve was 16.5% lower (Fig. 2 (a)). The measured power coefficient (C_P) vs. tip speed ratio (λ) curve showed a large scatter and varied significantly with temperature due to the pitch control of the turbine (Fig. 2 (b)).

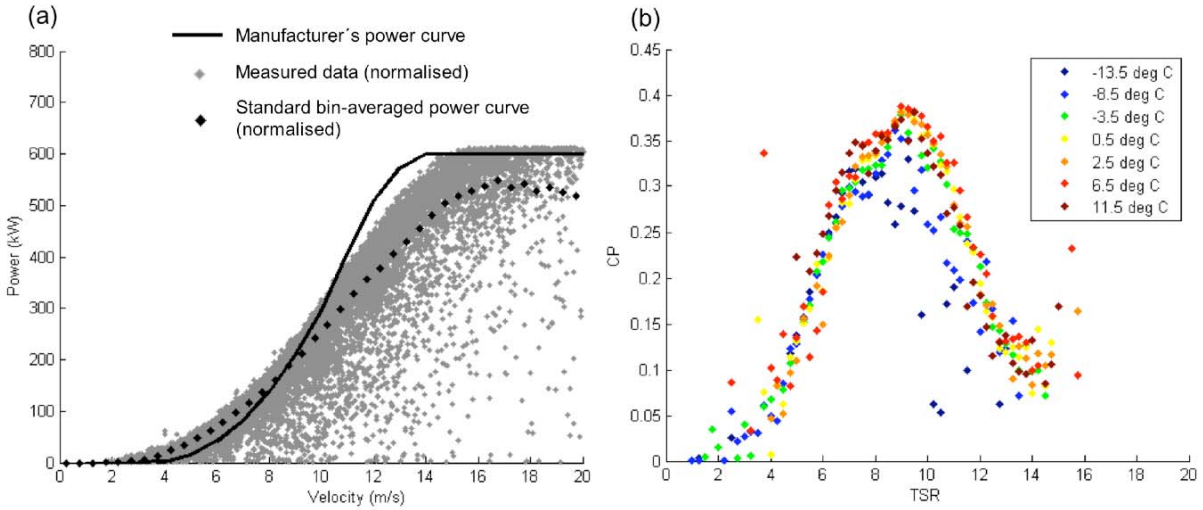

Figure 2. (a) Measured data and bin-averaged power curve compared to manufacturer's curve; (b) Bin-averaged power coefficient vs. tip speed ratio for measured data.

The calculated Annual Energy Production (AEP) was 2.3% lower than the actual production, and the capacity factor was low at 0.15. The AEP prediction using the manufacturer's density-corrected power curve was 20% lower. Since this method is used widely in the planning phase of a project, such a deviation could be highly problematic for wind farm developers and investors.

Analysis based on temperature bins showed that the power production was particularly high when ambient temperatures were between -5 and 15 ^{o}C, and the energy production particularly high with temperatures between -1 and -9 ^{o}C (Fig. 3 (a)). As can be seen in Fig. 3 (b), this cannot be explained directly by the high velocity at these temperatures.

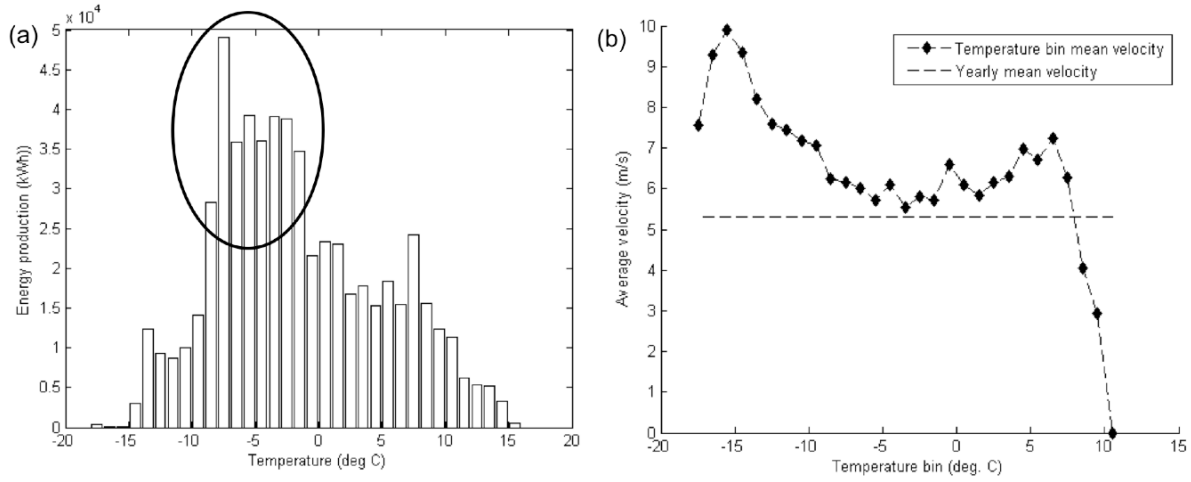

Figure 3. (a) Energy production bin-averaged with temperature; (b) Velocity bin-averaged with temperature.

The temperature at this site has a large influence on AEP; a 50% reduction in AEP was estimated if the wind conditions would remain at the 10 ^{o}C average velocity for the entire year. The wind conditions at low temperatures are clearly highly beneficial to AEP.

The direct effects of ice formation were analysed by correlating photographs of the blades from the nacelle of the turbine with the measurement data. The data at the points where icing was detected were replaced with the average monthly power values that would have occurred if the icing points were not included. Icing was estimated to cause a 12.1 MWh (1.6%) reduction in yearly energy production, 8.4 MWh of which was directly caused by ice on the blades. The majority of the losses seen in the measured power (Fig. 2 (a)) were thus attributed to other effects such as turbulence and wind gusts, which should be further investigated.

In summary, despite the detrimental effects of ice formation, the development of wind farms in alpine environments can be highly beneficial due to the favourable wind conditions. At the Alpine Test Site Gütsch, the improvement in energy yield at low temperatures is significantly higher than the detrimental effect of ice formation on the blades. However, this can vary greatly between sites, and the direct effects of different ice sizes and shapes on the blades must be better understood in more detail. Furthermore, the detrimental effects of phenomena such as turbulence and wind gusts should be further investigated.

In the remainder of this work, the effects of different ice shapes on the power production of a wind turbine in a controlled test environment (Section 3) and using Compuational Fluid Dynamics (Section 4) are systematically investigated. The ice shapes are defined in the following section.

2.2 Definition of ice shapes

The aim of this part of the work was to define ice shapes representative of those formed on full-size, in-situ wind turbines. The ice shapes previously defined in the Halfway Report (Barber, 2009) were improved by combination of a photograph analysis technique with an ice accretion code. The new shapes are summarised in Fig. 4. The span-wise distribution refers to the span-wise extent of icing measured from the blade tip.

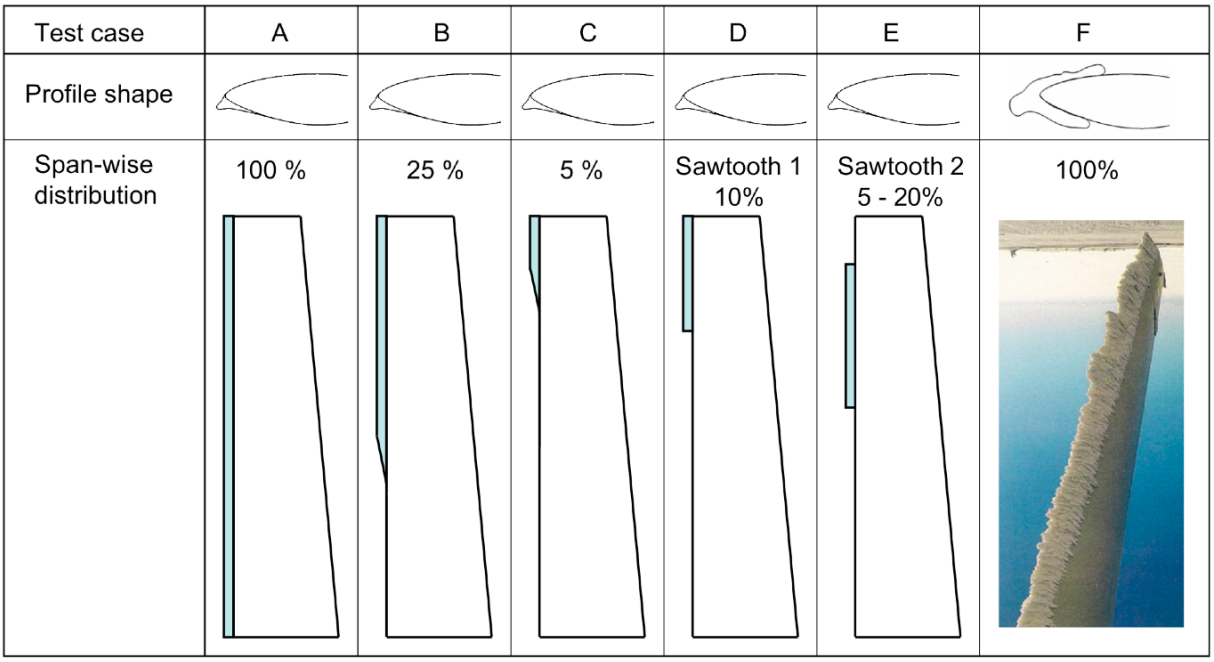

Fig. 4. Defined ice shapes.

The photographs provided an approximate span-wise distribution of ice accumulation and served as a reference for the validation of simulated ice shapes. The 2D NASA-LEWICE ice accretion code was used to calculate the flow field around blades and provided detailed 2D ice profiles. This combined use of photographs and ice accretion code thus enabled the reproduction of detailed 3D ice shapes.

LEWICE was used to predict 2D ice profile shapes on the blades at eight different span-wise locations. The other input parameters, as shown in Table 1, were selected using the conditions at the Alpine Test Site Gütsch. The wind parameters were taken as the average values for the measurement data described in Section 2.1. In order to estimate the liquid water content, simulations using the weather forecast model WRF (Skamarock *et al.*, 2005) were carried out by Meteotest for a typical icing event at Gütsch. The chosen droplet diameter was estimated based on previous LEWICE simulations (Broeren *et al.*, 2006).

Table 1. Parameters used to define icing profiles.

Turbine diameter	44 m
Turbine rotational speed	15 rpm
Wind velocity	4 m/s
Temperature	-6 °C
Liquid water content	0.1 g/m^3
Droplet diameter	35 µm
Icing duration	10 hours

The LEWICE results for span-wise distances r/R = 0.30, 0.63 and 0.90 are shown in Fig. 5. The shape grows with increasing span due to the increasing rotational ($r\omega$) component of the velocity and decreasing angle of attack (α).

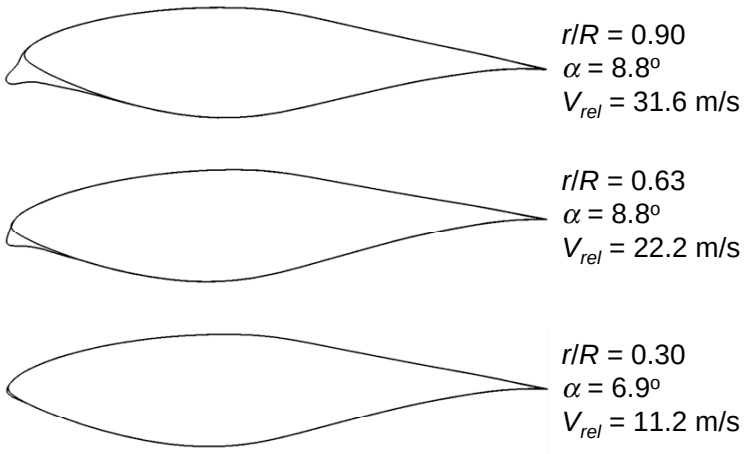

Fig. 5. Predicted ice profiles at three span-wise locations.

The results from LEWICE were used in conjunction with photographs from the Alpine Test Site Gütsch. Approximately 11,000 photographs from a camera mounted on the nacelle of the wind turbine taken over the period between 01/06/2007 and 31/05/2008 were analysed to establish typical span-wise distributions. It should be noted that the blades on the turbine at Gütsch are fitted with air heating systems, which are activated if the power output reaches unacceptably low values in cold temperatures. This means that the ice profiles are not extreme.

Once span-wise ice distributions were established and the 2D profile shapes were predicted in LEWICE, five ice shapes (Cases A-E) were defined for the tests. Cases A-C represent varying length of span-wise ice formation, which result from the varying tip speed ratio conditions of the wind turbine. In each the ice shape was case linearly tapered to avoid sharp steps. Cases D and E represent the “saw-tooth” effect that was frequently observed in the photographs. This occurs when parts of the ice falls off the blade during motion. These shapes were made intentionally with sharp steps. An example photograph from Gütsch is shown in Fig. 6 compared to the CAD drawing for Case A. The view angle is the same as the camera angle.

The final ice shape (Case F) is an extreme case that was not observed at Gütsch, but at a site where no heating system is present (Grenchenberg, Switzerland).

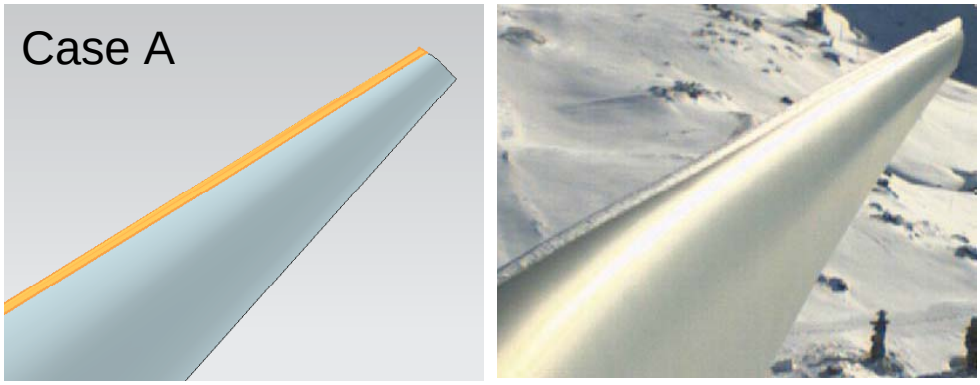

Fig. 6. Comparison of Case A with a photograph from Gütsch.

3. Sub-scale measurements

In the second part of the project, a new sub-scale model wind turbine test facility was set up and a novel power measurement technique developed. The performance was measured and assessed for a wind turbine with no ice and with the six defined ice shapes attached to the blades. Following the provision of additional support from BFE in December 2008, a Fast-Response Aerodynamic Probe (FRAP) measurement system was also integrated into the sub-scale model test facility.

3.1 Sub-scale model wind turbine test facility

The design and set-up of the new facility can be found in more detail in Barber, 2008. The facility is pictured in Fig. 7 (a). It comprises a 0.3 m diameter wind turbine model mounted on a carriage that moves above a 40 m long, 1 m wide and 1 m deep channel of water. The velocity of the carriage can be specified to up to 3 m/s (± 1%), as shown schematically in Fig. 7 (b). The water temperature is at 19 ^{o} ± 0.5 ^{o} throughout the measurement campaign. The blockage ratio ($A_{rotor}/A_{channel}$) of the model is 7.1%, which is below the upper limit of 7.5% that is required to apply blockage corrections (Rae *et al.*, 1999). The wind turbine tower is inside a streamlined section, whose Froude number for surface waves of 1.9. Thus surface and blockage effects have a negligible effect on the wind turbine performance.

The rotor blades are interchangeable and the pitch angle can be set to ± 2 ^{o}. For the current tests the blade pitch was 0 ^{o}. The blades match the twisted and tapered NREL Phase VI rotor from 25% span outwards. The rotational speed of the wind turbine is controlled by a brushless motor. The desired tip speed ratio of the wind turbine can thus be accurately specified. In this study, the turbine rotational speed was kept at 800 rpm (± 3 rpm), which avoided cavitation on the blades. The tip speed ratio was varied from 5 to 8 by varying the carriage velocity between 1.5 and 2.8 m/s.

The Reynolds number based on mean chord at the optimal tip speed ratio of 6.0 is about 1.4 x 10^5 in this facility. As a comparison, the same size model in a wind tunnel would reach a Reynolds number of 10,000. The largest wind tunnel facility used for wind turbine testing (at NASA-AMES) has Reynolds numbers of the order of 9.1 x 10^5. At Gütsch the Reynolds number is approximately 4.0 x 10^6. It is evident that this facility enables the full-scale non-dimensionals to be better duplicated on the sub-scale model than in air.

3.2 Performance measurement technique

To determine the performance of the wind turbine, an in-line, contactless miniature torquemeter with measurement range 0-5 Nm (accuracy ± 0.1%) was installed on the shaft. This is a significant improvement on the previous technique described Barber, 2008, and avoids the use of two ambiguously specified calibration factors.

Torque was converted to power by multiplying it by the rotational speed. The power of the turbine, P_{turb}, measured in the water channel, is comprised of the power required by the motor to overcome friction in the drivetrain, P_{drive}, the dynamic sealing, P_{seal}, and the power absorbed by the rotor itself, P_{rotor}, which is negative for a wind turbine:

$$P_{turb} = P_{drive} + P_{seal} + P_{rotor} \tag{1}$$

Or for constant rotational velocity, ω:

$$T_{turb} = T_{drive} + T_{seal} + T_{rotor} \tag{2}$$

where T = torque (N/m^2). As shown in Fig. 8, the measurement of T_{turb} in the water channel requires also a series of tare measurements in order to determine T_{drive} and T_{seal}.

This approach assumes that the parasitic torque componenets due to the seal and the housing are decoupled from each other and from the torque produced by the blades. Once T_{rotor} was established for each case, the power coefficient was determined as follows:

$$C_P = \frac{T_{rotor}\omega}{\frac{1}{2}\rho V^3 A_{rotor}} \tag{3}$$

where A_{rotor} is the cross-sectional area of the rotor (m), V the carriage velocity (m/s) and ρ the fluid density (kg/m^3).

The relative errors of the C_P and tip speed ratio measurements were calculated using the stated percentage errors in the translational velocity (± 1%), rotational velocity (800 rpm ± 3 rpm), torque (± 0.1%) and water temperature (19 ^{o} ± 0.5^{o}). The worst case relative errors were found to be 3.0% in C_P and 1.1% in tip speed ratio.

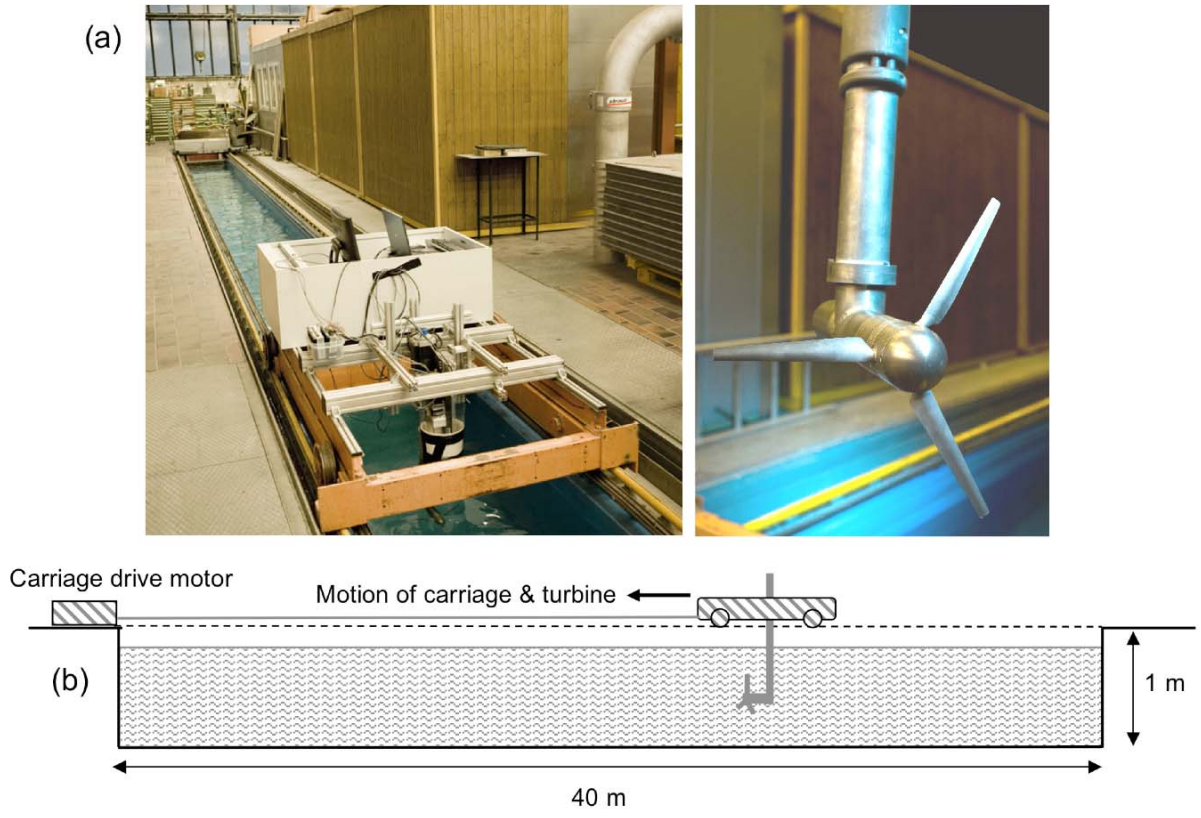

Fig. 7. Sub-scale model wind turbine test facility, (a) photograph, (b) schematic diagram.

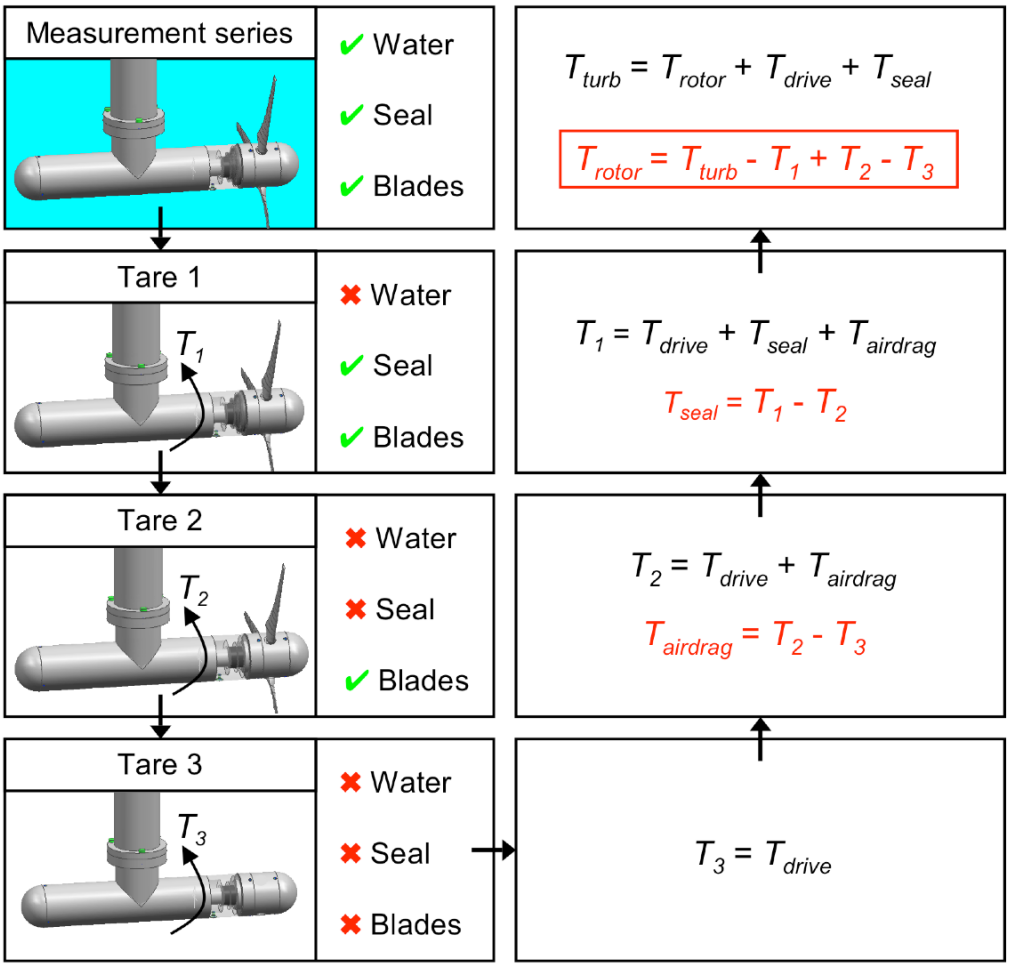

Fig. 8. Torque measurement method.

3.3 Reynolds number correction

As noted above, the dynamically-scaled model in the present work better duplicates the full-scale Reynolds number than in a wind tunnel. However the measured power coefficient must be corrected to account for the Reynolds number difference between the sub-scale model and a full-scale turbine. A Reynolds number correction was therefore developed as described next. The skin friction coefficient for turbulent flow (c_{fT}) over a flat plate is defined as follows [10]:

$$c_{fT} = \frac{0.074}{\mathrm{Re}_T^{0.2}} \tag{4}$$

where Re_T is the local blade Reynolds number. Thus the corrected power coefficient is given as the following:

$$C_P = \frac{c_{f\,\mathrm{Re}!}}{c_{f\,\mathrm{Re}}} C_P! \tag{5}$$

where $C_P!$ is the uncorrected power coefficient, Re the full-scale Reynolds number and Re' the sub-scale Reynolds number. A comparison of measurements of a 2-bladed sub-scale model in the ETHZ facility (Re' = 1.44 x 10^5) and the NREL Phase VI test case [9] (Re = 9.06 x 10^6) is shown in Fig. 9. The two measurements have an average difference of 5%, which confirms the Reynolds number correction that is developed here. The differences are

attributed to the small differences in the hub geometry and nose cone shape between the sub-scale and NREL configurations.

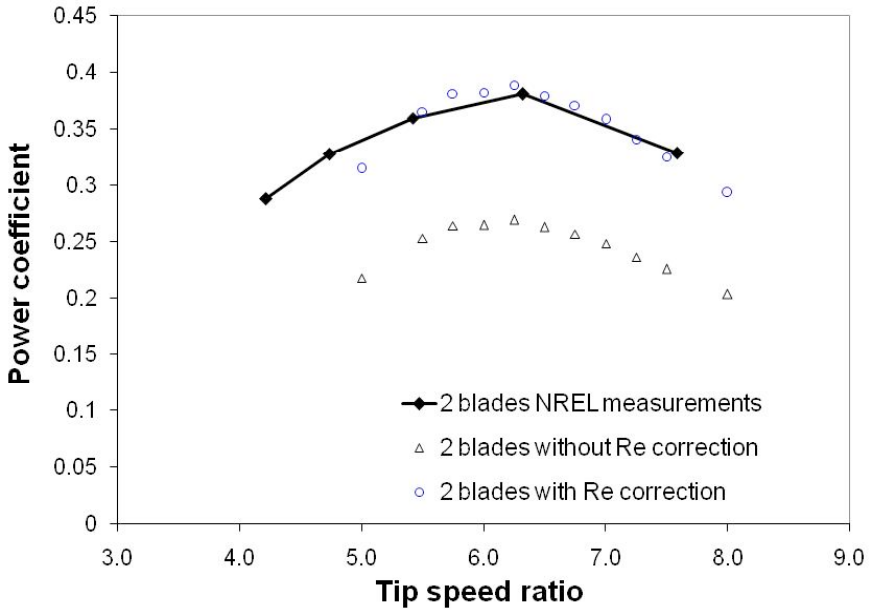

Fig. 9. Power coefficient vs. tip speed ratio (2-bladed rotor).

3.4 The effect of ice shapes on performance

Baseline power coefficient curves (no icing)

The power coefficient vs. tip speed ratio curve for the clean blades (no ice) is shown in Fig. 10. The shape is as expected for a 3-bladed wind turbine, with a peak at a tip speed ratio of approximately 6.0 – 6.5, where the power coefficient is 0.33. Repeat measurements showed very good repeatability and a maximum variation in C_P of 1.7%, which is within the relative error of the experiment (section 3.2).

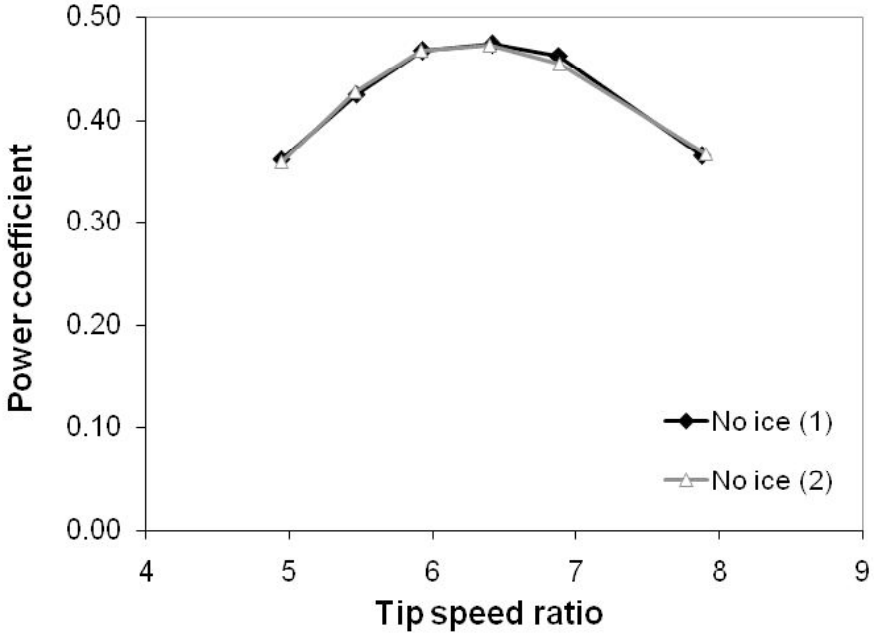

Fig. 10. Power coefficient vs. tip speed ratio graph, rotor with no ice.

Power coefficient curves (icing conditons)

The effect of icing on the wind turbine performance is shown in Fig. 11 (a) for Case A, B & C and (b) for Case D, E & F. Additionally, the relative magnitudes of C_P are examined further in Fig. 12, in which ΔC_P (the difference between C_P with ice and with no ice) for the Cases A-E for selected tip speed ratios are compared. Case F is not included for sake of clarity.

It can be seen that the presence of the ice generally has a detrimental effect on the performance of the rotor. The reduction of C_P is as large as 0.08 (or 29.3%) for Cases A and B. The effect is smaller at lower tip speed ratios, and all the C_P values are within 0.015 of each other by a tip speed ratio of 4.9. This trend is expected because the losses at high tip speed ratio are mainly dictated by the aerodynamic drag of the blades, whereas the losses at low tip speed ratio are dominated by the wake angular momentum losses. The aerodynamic drag of the blades is expected to be altered due to the ice shapes, whereas the wake losses are less sensitive to blade profile and tip speed ratio. Thus the ice shapes are expected to alter C_P more significantly at higher tip speed ratios.

On examination of the uniform ice shapes (Cases A-C), it can be seen that C_P is reduced by up to 29.3% (at tip speed ratio = 7.9) for the 100%-span ice shape (Case A). The 25%-span ice shape (Case B) shows very similar behaviour, the maximum difference from Case A being 2.6% at tip speed ratio = 7.9. This suggests that only the ice in the outboard 25% of the span has a significant effect on performance. Furthermore the reduction in performance measured for the 5% case (Case C) is approximately half that of the 25% case for the tip speed ratios close to the maximum. This means that the presence of ice on the outboard 5% of the blade has a similar impact on performance as ice on 75% to 95% of the span. This indicates a rapidly increasing effect on performance from ice that is nearer the tip. Thus ice removal or prevention systems could be substantially more efficient if their effectiveness was tailored to the outboard 5% span of the blades.

Cases D and E show the effects of the two “sawtooth” shapes on the turbine performance. Ice Case D consists of one sharp step from the ice shape to the blade surface at 10% span. This has a very similar effect on performance as the 5% span tapered ice shape (Case C). Case E has two sharp steps from the blade to the ice shape on either side at 5% and 25% span. This ice shape has a larger influence on C_P at high tip speed ratios (C_P is 7.4% larger for Case E than for Case D at a tip speed ratio of 6.9). This again highlights the strong effect of ice that is on the outboard 5% span.

The extreme ice shape, Case F, has a major effect on the C_P. No power is generated for tip speed ratio > 6, and the power is small for tip speed ratio < 6.

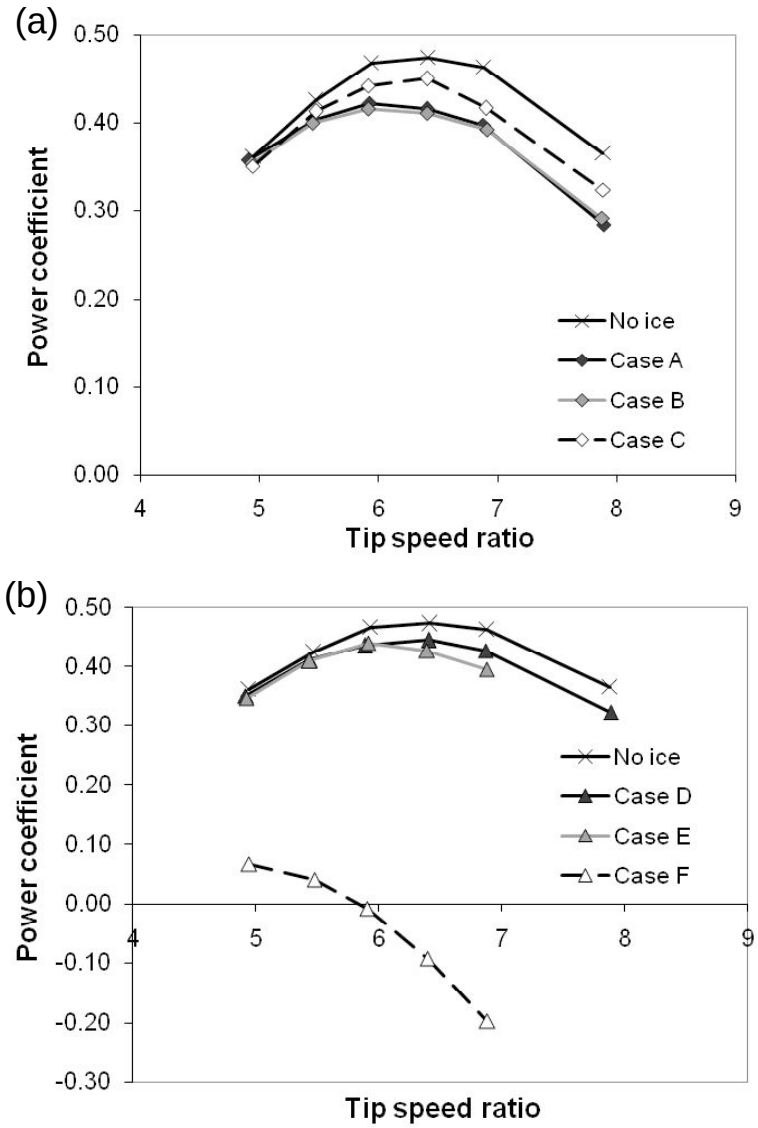

Fig. 11. Power coefficient vs. tip speed ratio graph for the rotor with ice shapes attached to blades: (a) Cases A-C compared to no ice case, (b) Cases D-F compared to no ice case.

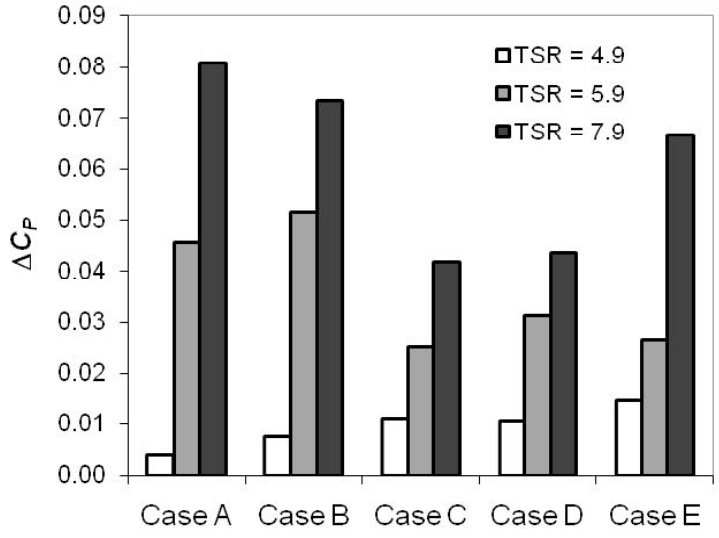

Fig. 12. ΔC_P for Cases A-E for various tip speed ratios.

Annual Energy Production

The potential effects of the ice shapes on the corresponding Annual Energy Production (AEP) of a wind turbine were estimated using the atmospheric conditions at Gütsch. A continuous operation at a tip speed ratio of 5.9 (and thus the corresponding C_P measured in the above experiments) was assumed. The resulting power curves for the clean blades and for Case A are shown in Fig. 13, where the air density was taken as 1.225 kg/m^3 and the curve was cut off at the rated power of 600 kW to simulate pitch control.

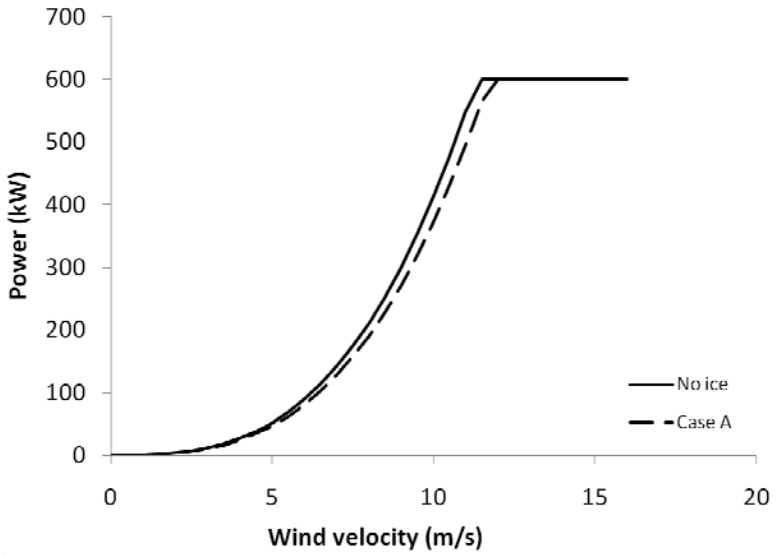

Fig. 13. Estimated power curves for the clean rotor and Case A.

The AEP was estimated using the IEC standard bins method (IEC, 1998), where ε(v) = power curve and $f_{ref}(v)$ = measured wind speed frequency distribution over a year at the test site Gütsch:

$$AEP = \int_0^\infty \varepsilon(v) f_{ref}(v) du \tag{6}$$

The resulting AEP for each case is summarised in Table 2, for icing 100% of the time and for icing for only two months of the year. The two month long period was estimated as the duration of likely ice formation based on temperature data measured at Gütsch over a year together with LEWICE simulations for a range of temperatures and humidities.

Table 2. Effect of Ice on Annual Energy Production.

	12 months icing		2 months icing	
Case	AEP (MWh)	% loss	AEP (MWh)	% loss
Clean	181	-	181	-
Case A	163	9.7	178	1.6
Case B	161	11.0	177	1.8
Case C	171	5.4	179	0.9
Case D	169	6.7	179	1.1
Case E	170	5.7	179	0.9
Case F	0	100	151	16.7

In the full-scale measurement data analysis summarised in Section 1.1, the actual loss in AEP at Gütsch due to ice formation over a year was estimated to be approximately 1.1%, which is good general agreement with that of Cases A-E here. Case F, which is representative of ice formation of example in the Bern Jura, clearly has a much more deleterious effect (17% less) on the AEP.

3.5 FRAP measurements

System set-up

A dedicated measurement system using the laboratory's in-house developed Fast Response Aerodynamic Probe (FRAP) system was set up for the sub-scale model wind turbine test facility. The steps undertaken in the design and integration of this system were discussed in detail in Barber, 2009. The FRAP system allows detailed, time-resolved flowfield measurements to be made behind the model wind turbine rotor in controlled test conditions. This enables assessment and comparison of the flow features that are responsible for power production and performances losses in different wind and atmospheric conditions.

The probe tip has a diameter of 1.8 mm and two miniature silicon pressure transducers are placed directly in the head. The system consists of the measurement probe itself plus cables for signal transfer, a Power Pressure Unit to supply the correct pressure air to the probe, a PC & data processing software, a traversing system used to position the head of the probe in three axes to the nearest 0.1 mm and a trigger system to identify the blade position and the rotational velocity. The measurement data is saved onto a portable hard drive in a format suitable for the laboratory's in-house data processing tool.

The mechanical set-up of the 3-axis traversing system that was recently installed in the facility is shown in Fig. 14. It can be positioned by the computer using dedicated control software in a 800 mm vertical range, a 500 mm horizontal range and a 360 ^{o} rotational range.

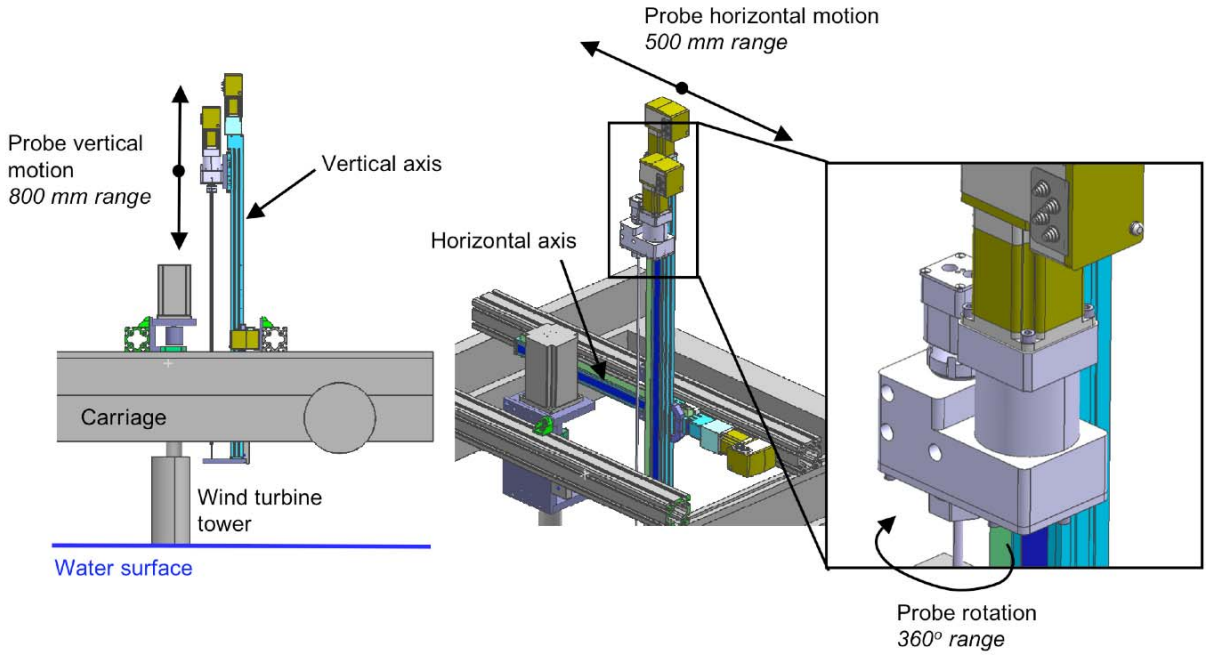

Fig. 14. Mechanical set-up of traversing system.

Results

The new FRAP system was used to examine the flow in a plane 30 mm behind the sub-scale model wind turbine rotor. The rotor was operating at its optimal tip speed ratio of 6. Measurements in the freestream give a turbulence intensity of 0.04%.

Measurements were made over 4 seconds at 10 different radial points in a vertical line directly behind the rotor. For each measurement point the 3D velocity, flow angles and total pressure were measured at a frequency of 10 kHz, and the data was phase locked averaged over 52 revolutions of the rotor. An example of the calculated, phase locked averaged total velocity at one measurement point close to the blade tip (r = 150 mm) is shown in Fig. 15. As expected the passage of the tip vortex can be clearly seen to occur three times per revolution.

The results for all the measurement points are shown in Fig. 16 in terms of (a) total velocity and (b) total pressure. These measurements demonstrate the unique capability that has now been developed in the ETHZ sub-scale wind turbine test facility.

These results show the expected periodic behaviour due to the presence of the three rotor blades. The vortex formation off the tip of each blade, as well as a low pressure wake region directly behind the blades, are clearly indentifiable. Furthermore, the periodic, low-velocity region in the wake can be clearly seen. The presence of a hub vortex can be identified even though in this measurement campaign the probe was not lowered any nearer to the hub. Analysis of the flow angles and velocity components are currently underway. Further measurement campaigns under a range of operating conditions will also be conducted.

It is clear that this measurement system records flow fields to the required accuracy to allow the assessment and comparison of flow phenomenon under different conditions in the sub-scale test facility. The unique capability of the ETHZ sub-scale wind turbine test facility is evident here.

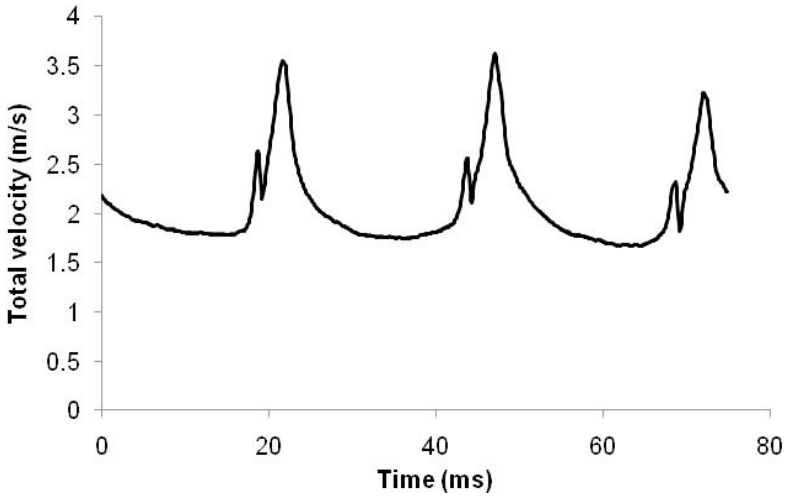

Fig. 15. Phase locked averaged total velocity at r = 150 mm.

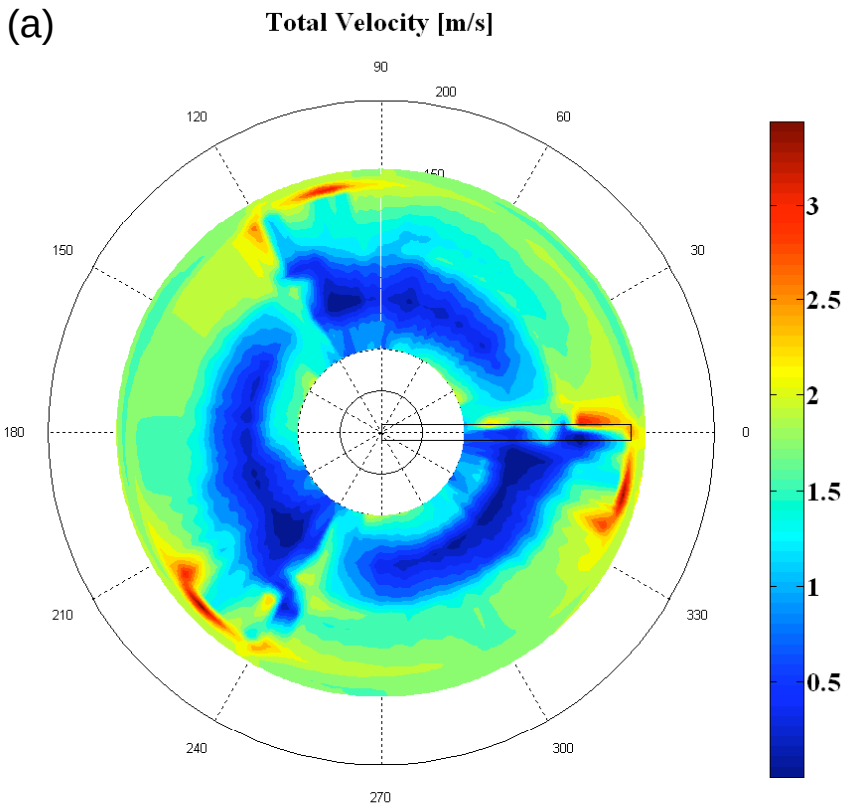

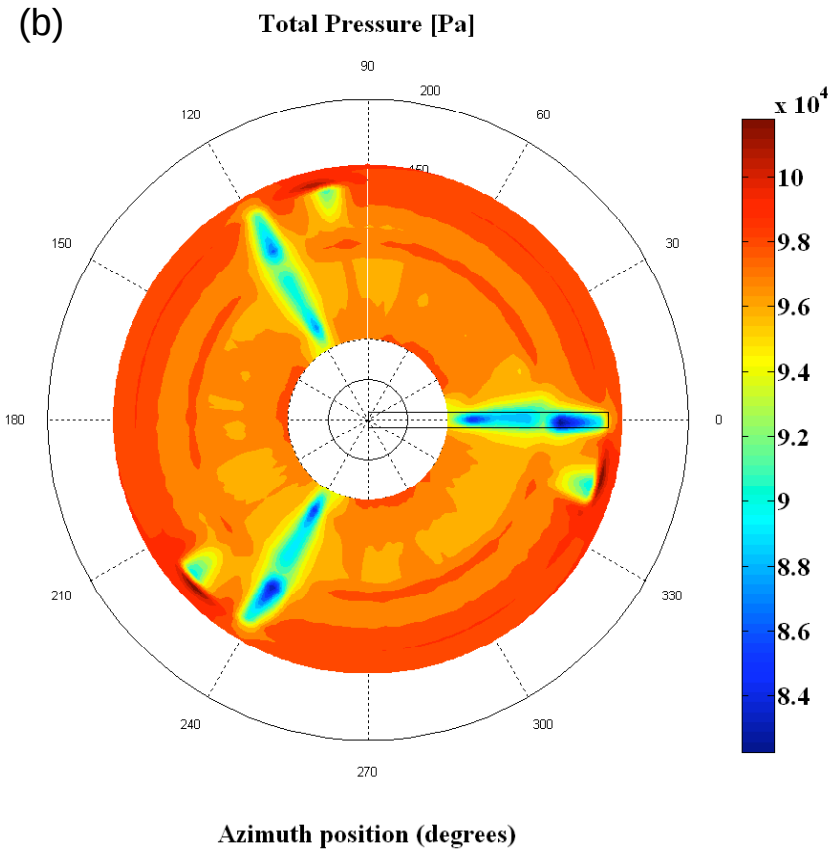

Fig. 16. Results: (a) Total velocity, (b) Total pressure.

4. Computational Fluid Dynamics

The third part of the project involves the CFD analysis of the wind turbine rotor with and without ice shapes attached. The detailed design and set-up of the mesh and boundary conditions were described previously in Barber, 2008 and Barber, 2009.

4.1 Summary of set-up

The commercial code ANSYS CFX 11.0 was used to perform the CFD analysis. A single blade was analysed with periodic boundaries as shown in Fig. 17. Due to constraints in computational power the study was limited to a 120 ^{o} arc-shaped domain of radius 4*R* and length 4*R*.

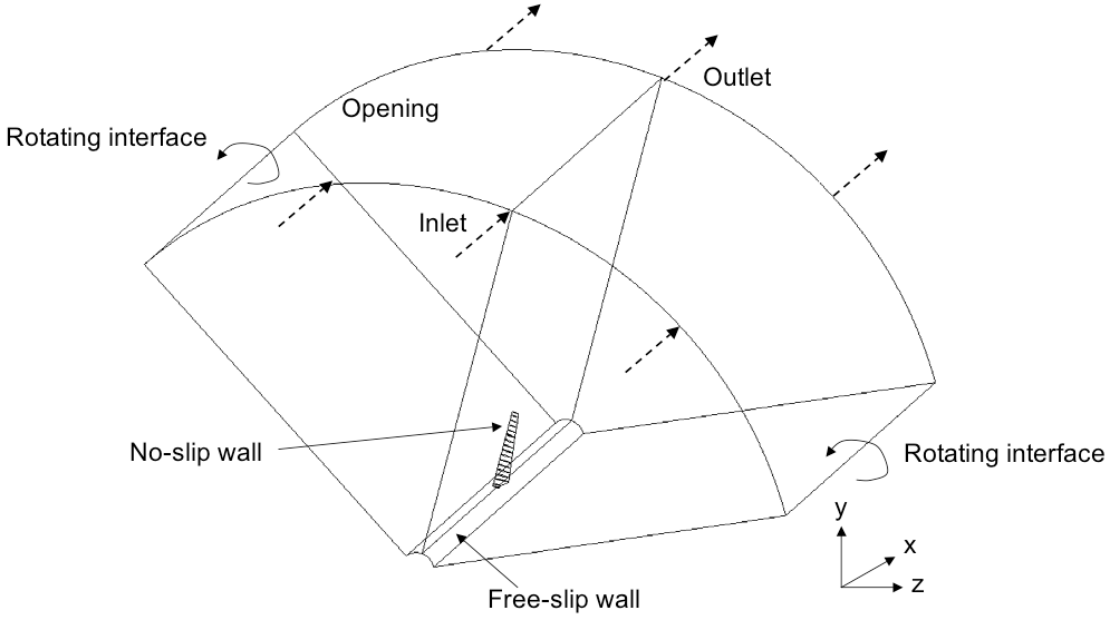

Fig. 17. Computational domain.

An unstructured tetrahedral mesh was constructed in the domain with 10 prism layers on the surface of the blade. It was ensured that at least 10 cells were in the boundary layer, a requirement for the deployment of the scalable wall function with the k-ε turbulence model. The y^+ value on the blade surface remained consistently between about 30 and 60. A denser region of cells was constructed in the rotor wake. The grid dependency study included altering the cell sizes on the boundary surfaces region, the wake region and in the prisms close to the blade surface, until grid independent solution was found. The resulting mesh contained approximately 4 million cells. Convergence was considered adequate once the average residuals had decreased by five orders of magnitude.

As in the experimental study, the rotational velocity of the rotor was 800 rpm and the inlet velocity was varied. The boundary conditions are summarised in Table 3.

Table 3. CFD boundary conditions.

Inlet	v = 1.6 – 3.1 m/s
Outlet	Constant pressure
Top	Constant pressure opening
Bottom	Free slip wall
Blade	No slip wall
Periodic boundaries	800 rpm

4.2 The effect of ice shapes on performance

The steady-state results of the CFD simulations are presented next. For the examination of the performance due to the ice shapes, the behaviour at a tip speed ratio of 6.0 was considered. This operating point is the main region of interest particularly for variable speed wind turbines as at Gütsch. The C_P results were corrected for Reynolds number as in Section 3.3. In Fig. 18 the predicted ΔC_P values are shown for cases A-E (tip speed ratio = 6.0) compared to the experiment (tip speed ratio = 5.9). The case-to-case trends in the predictions match the experimental measurements well for all cases (within a ΔC_P value of 0.009 of each other, or 2.5% of the measured C_P). Case F reduces C_P to zero in both cases (100% loss).

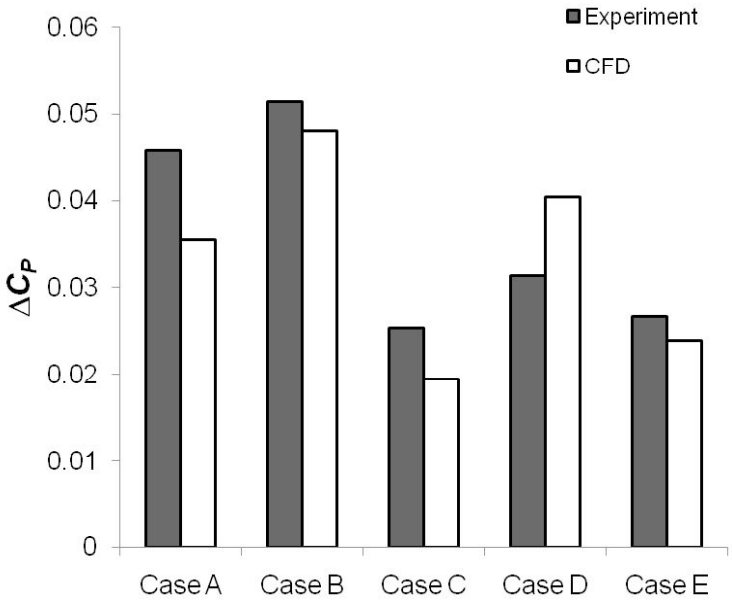

Fig. 18. ΔC_P for Cases A-E for CFD (tip speed ratio = 6.0) and experiment (tip speed ratio = 5.9).

The predicted streamlines, Fig. 19, show that there is no significant difference between the streamlines for the blade with no ice and for Case A and thus Case A does not significantly alter the characteristics of the separation. The only region of separation is at the hub. This flow behaviour was also observed for Cases B-E, and explains why the measured CP values are all of the same order. However, Case F has massive amounts of separation across the span. This explains the total loss in power seen for this tip speed ratio for Case F.

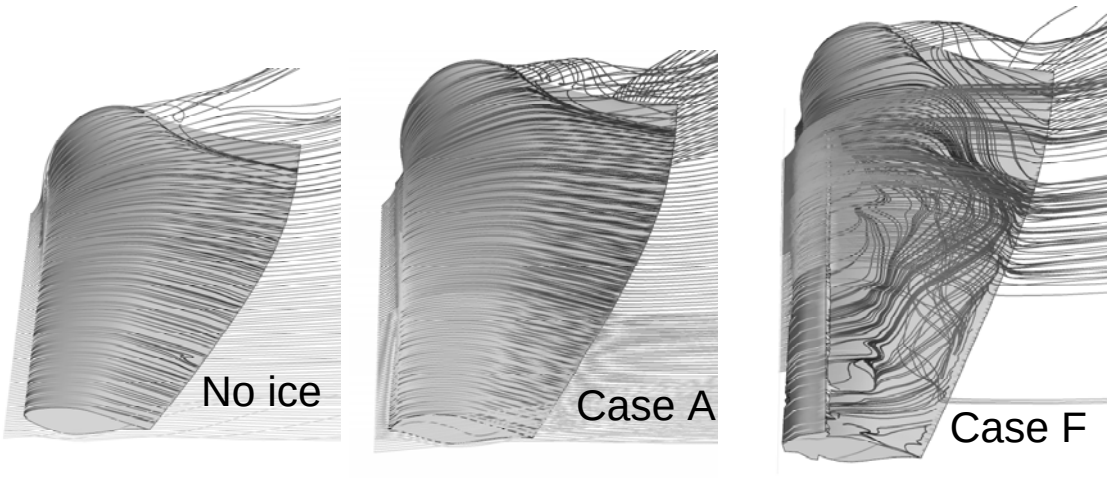

Fig. 19. Streamlines over the blade for Cases A & F compared to no ice.

5. Discussion and recommendations

5.1 Non-“extreme” ice

This work has shown that ice experienced by the wind turbine at the Alpine Test Site Gütsch does not cause significant losses in power and AEP (up to 2%). The actual losses in power of the Gütsch turbine are, however, much larger. This can be seen in the comparison between the manufacturer’s power curve and the actual power curve in Fig. 2(a). The differences between the manfacturer’s and actual power curves show a loss of AEP of 23%. These large losses in AEP are attributed to the high turbulence and wind gusts found in the complex terrain at the Gütsch site. These losses must be investigated further.

5.2 “Extreme” ice

It was found that “extreme” ice shapes that are large enough to cause flow separation over the entire blade can be responsible for significant power losses and reduce the AEP by an order of 20%. This type of ice may be expected to form at altitudes in the range 800 – 1500 m such as the Bern Jura. It is thus key for wind farm developers to be able to predict the likelihood of “extreme” ice forming on the blades at planned locations.

The next steps of this study are therefore to (i) define quantitatively the characteristics of “extreme” ice and (ii) combine this definition with an icing event prediction model such as the Weather Research & Forecasting model of Meteotest. Icing event prediction models are required because the likelihood of icing events depends on a number of different factors. For example, even though the Gütsch site is at an altitude of 2331 m, only small amounts of ice form on the blades. However, the Grenchenberg site is at a lower altitude of 1350 m but it subject to “extreme” icing due to the particular combination of temperature and humidity conditions there. Ultimately it is anticipated that this work will result in a predictive tool that developers of wind energy projects located in regions that are highly susceptible to icing can use for project development.

5.3 Icing mitigation

It was shown that non-“extreme” ice that forms on the blades up to 75% blade span does not affect the performance of the turbine. Futhermore, the detrimental effect of icing increases rapidly from 75% to 100% blade span. The outboard 5% of the blade span was identified as the key area where the presense of ice most significantly decreases the performance.

Current blade heating systems blow hot air through the entire blade and their effectiveness reduces with increasing span. They are thus highly inefficient for such an application. It is recommended that heating systems should specifically target the outboard 5% of the blade in a localised manner such as with electric heating.

6. Conclusions

In this first part of this project, atmospheric, wind and power measurements over a year at the Alpine Test Site Gütsch were analysed. The following conclusions were drawn:

- Icing caused a reduction in Annual Energy Production of approximately 12.1 MWh (1.6%), 8.4 MWh of which was directly caused by ice on the blades.
- The Annual Energy Production at Gütsch was 23% lower than predicted with the manufacturer’s density-corrected standard power curve; this was attributed to external effects specific to the complex terrain such as high turbulence and wind gusts.
- The power production was particularly high when ambient temperatures were between -5 and 15 ^{o}C, and the energy production particularly high with temperatures between -1 and -

9 ^{o}C; a 50% reduction in annual energy production was estimated if the wind conditions would remain at the 10 ^{o}C average velocity for the entire year.

The second part of the project involved the set-up and development of the sub-scale model wind turbine test facility at ETH Zürich. A novel method for performance measurements was developed and a Fast-Response Aerodynamic Probe system installed. The facility has been shown to be capable of testing dynamically scaled models at near full-scale non-dimensionals. The unique capabilities of this facility were demonstrated in the study of the effect of icing on wind turbine performance, where the following conclusions were made:

- Ice formed at the high altitude atmospheric conditions of the Alpine Test Site Gütsch (2330 m) can reduce the Annual Energy Production by up to 2%.
- At lower altitudes typical of the Bern Jura (800-1500 m), the formation of ice on the blades can reduce the Annual Energy Production by up to 17%.
- For ice typical of that at high altitudes, the ice on the outboard 25% of a blade's span has a significant impact on performance. The ice on the most outboard 5% of the blade has as much adverse impact on performance as the ice on 75-95% span.
- Ice removal or prevention systems could be substantially more efficient if their effectiveness was tailored for the outboard 5% of the blade.

In the third part, an accompaning CFD study was undertaken, and the reduction in performance due to the ice shapes matched well with the experimental measurements. The more extreme ice formed at lower altitudes was found to reduce the performance drastically due to flow separation over the span of the blades.

It was recommended that wind turbine blade heating systems should specifically target the outboard 5% of the blade in a localised manner such as with electric heating. Furthermore, this work could be used to develop a predictive tool that planners of wind energy projects located in regions that are highly susceptible to icing can use for project development.

Personnel and acknowledgements

The additional personnel working on this project were:

- Samira Jafari, PhD student, LEC.

The authors would like to thank the LEC workshop and in particular Cornel Reshef and Thomas Künzle for their technical help in the project, René Cattin (Meteotest) & Markus Russi (Elektrizitätswerk Ursern) for access to the data as well as Silke Dierer for providing WRF simulation data. Thanks also to Katja Maus and the BFE for supporting the project and enabling it to take place.

References

Barber S (2008) Development of wind turbines for safe operation in alpine environments, BFE End of Year Report.

Barber S (2009) Development of wind turbines for safe operation in alpine environments, BFE Halfway Report.

Bose N (1992) Icing on a small horizontal-axis wind turbine – Part 1: Glaze ice profiles, *Journal of Wind Engineering and Industrial Aerodynamics* **45**, pp. 75-85.

Bragg M, Broeren A, Addy H, Potapczuk M, Guffond D, Montreuil (2007) Airfoil ice-accretion aerodynamics simulation, *45th AIAA Aerospace Sciences Meeting and Exhibit*, 8-11 January 2007, Reno, Nevada.

Brahimi MT, Chocron D and Paraschivoiu I (1997) Prediction of ice accretion and performance degradation of HAWT in cold climates, *AIAA-98-0026*.

Broeren AP, Bragg MB and Addy HE (2006) Flowfield measurements about an airfoil with leading-edge ice shapes, *Journal of Aircraft* **43** (4), pp. 1226-1234.

Hau E (2006), *Wind Turbines*, 2nd ed., Springer Verlag.

IEC Wind Turbine Generator Systems, Part 12: Power Performance Measurement Techniques (1998), *IEC International Standard 61400-12*.

Rae WH, Pope A and Barlow JB (1999), *Low-Speed Wind Tunnel Testing*, 3rd ed., John Wiley & Sons.

Schlichting H (2000), *Boundary-layer theory*, 8th ed., Springer Verlag.

Skamarock WC, Klemp JB, Dudhia J, Gill DO, Barker DM, Wang W and Powers JG (2005), A description of the advanced WRF version 2", National Center for Atmospheric Research, Boulder, CO, *Tech. Note NCAR/TN-468+STR*.